OPEN ACCESS Freely available online

PLOS ONE

Platelet Serotonin Transporter Function Predicts Default-Mode Network Activity

Christian Scharinger[1☯], Ulrich Rabl[1☯], Christian H. Kasess[1,3], Bernhard M. Meyer[1], Tina Hofmaier[2,4], Kersten Diers[5], Lucie Bartova[1], Gerald Pail[1], Wolfgang Huf[1,3,6], Zeljko Uzelac[4], Beate Hartinger[1], Klaudius Kalcher[1,3,6], Thomas Perkmann[2], Helmuth Haslacher[2], Andreas Meyer-Lindenberg[7], Siegfried Kasper[1], Michael Freissmuth[4], Christian Windischberger[3], Matthäus Willeit[1], Rupert Lanzenberger[1], Harald Esterbauer[2], Burkhard Brocke[5], Ewald Moser[3], Harald H. Sitte[4], Lukas Pezawas[1]*

1 Department of Psychiatry and Psychotherapy, Medical University of Vienna, Vienna, Austria, **2** Department of Laboratory Medicine, Medical University of Vienna, Vienna, Austria, **3** Center for Medical Physics and Biomedical Engineering, Medical University of Vienna, Vienna, Austria, **4** Center for Biomolecular Medicine and Pharmacology, Medical University of Vienna, Vienna, Austria, **5** Department of Psychology, Dresden University of Technology, Dresden, Germany, **6** Department of Statistics and Probability Theory, Vienna University of Technology, Vienna, Austria, **7** Central Institute of Mental Health, University of Heidelberg, Mannheim, Germany

Abstract

Background: The serotonin transporter (5-HTT) is abundantly expressed in humans by the serotonin transporter gene *SLC6A4* and removes serotonin (5-HT) from extracellular space. A blood-brain relationship between platelet and synaptosomal 5-HT reuptake has been suggested, but it is unknown today, if platelet 5-HT uptake can predict neural activation of human brain networks that are known to be under serotonergic influence.

Methods: A functional magnetic resonance study was performed in 48 healthy subjects and maximal 5-HT uptake velocity (V_{max}) was assessed in blood platelets. We used a mixed-effects multilevel analysis technique (MEMA) to test for linear relationships between whole-brain, blood-oxygen-level dependent (BOLD) activity and platelet V_{max}.

Results: The present study demonstrates that increases in platelet V_{max} significantly predict default-mode network (DMN) suppression in healthy subjects independent of genetic variation within *SLC6A4*. Furthermore, functional connectivity analyses indicate that platelet V_{max} is related to global DMN activation and not intrinsic DMN connectivity.

Conclusion: This study provides evidence that platelet V_{max} predicts global DMN activation changes in healthy subjects. Given previous reports on platelet-synaptosomal V_{max} coupling, results further suggest an important role of neuronal 5-HT reuptake in DMN regulation.

Citation: Scharinger C, Rabl U, Kasess CH, Meyer BM, Hofmaier T, et al. (2014) Platelet Serotonin Transporter Function Predicts Default-Mode Network Activity. PLoS ONE 9(3): e92543. doi:10.1371/journal.pone.0092543

Editor: Andreas Androutsellis-Theotokis, Universitätsklinikum Carl Gustav Carus an der Technischen Universität Dresden, Germany

Received December 27, 2012; **Accepted** February 25, 2014; **Published** March 25, 2014

Funding: This work was supported by the Special Research Project SFB-35 (Project No. F3514-B11, F3510-B11 and F3506-B11 to LP, MF and HHS, respectively) of the Austrian Science Fund (FWF) and the Institute for Study of Affective Neuroscience (ISAN) as well as by grants of the Austrian National Bank (OeNB P11903 to L. Pezawas and OeNB P13214 to R. Lanzenberger). The funders had no role in study design, data collection and analysis, decision to publish, or preparation of the manuscript.

Competing Interests: The authors have declared that no competing interests exist.

* E-mail: lukas.pezawas@meduniwien.ac.at

☯ These authors contributed equally to this work.

Introduction

The serotonin transporter (5-HTT) is abundantly expressed throughout the human body by the 5-HTT gene (*SLC6A4*). Highest amounts of 5-HTT protein can be found in the gastrointestinal tract, blood platelets, and serotonergic neurons in the brain [1]. In platelets, serotonin (5-HT) reuptake by transmembrane 5-HTTs represents the primary mechanism of 5-HT clearance from blood plasma [1]. Similarly, in serotonergic neurons, 5-HT reuptake by presynaptic 5-HTTs determines synaptic 5-HT levels [1]. The 5-HTT protein is therefore the central regulator of extracellular 5-HT levels in both platelets and serotonergic neurons [1,2]. In the brain, 5-HTTs are involved in numerous physiologic brain functions including emotion processing [2], which is known to be altered in major depressive disorder (MDD) [3]. The clinical efficacy of selective 5-HT reuptake inhibitors (SSRIs), the first-line treatment of MDD, constitutes the leading argument for the crucial role of 5-HT neurotransmission in depression [4,5].

Functional magnetic resonance imaging (fMRI) studies in depressed patients have contributed significantly to the biological understanding of neural changes in MDD [3,4,6,7]. However, due to obvious ethical limitations alterations of neural activation have so far not been directly associated with *in vivo* functional

assessments of the 5-HTT protein in humans such as maximal 5-HT uptake velocity (V_{max}). Nevertheless, indirect evidence of animal or human pharmacological studies suggests that 5-HTT function is modulating neural activation in brain centers that are detectable with fMRI and have been related to MDD [7,8,9,10,11,12,13,14,15]. Firstly, pharmacological MRI (phMRI) experiments in animals have demonstrated that drug-induced 5-HT challenge leads to changes in cortical activation [8,9]. Secondly, human phMRI studies revealed area-specific changes in BOLD signaling after SSRI administration [10,11,12,13,14,15,16]. Notably, short-term effects of pharmacologically increased 5-HT levels are involving a complex pattern of both BOLD signal increases and decreases in several cortical and subcortical brain regions that differ substantially from long-term effects [14,15,17]. Complementary, studies inducing a temporary reduction of 5-HT availability by dietary acute tryptophan depletion (ATD) have shown regionally specific effects on BOLD signaling [18,19].

The physiologic significance of those observations remains unclear since findings of pharmacological challenge studies cannot be directly applied to human neurobiology. Hence, alternative approaches such as multimodal imaging have been taken to elucidate the relationship between neural activation and physiologic 5-HT signaling *in vivo* in healthy humans [20,21]. While still rarely used, multimodal imaging studies have been able to relate BOLD signal changes of the amygdala and the default-mode network (DMN) to 5-HT receptor availability under physiologic conditions [20,21]. Moreover, one study found amygdala reactivity to be predictable by amygdalar 5-HTT availability [22]. Notably, no studies investigating the relationship between 5-HTT availability within the DMN and BOLD signaling are to our knowledge available today.

Importantly, positron emission tomography (PET) imaging does not allow for functional assessments of 5-HTT transport processes such as neuronal V_{max}, because it is confined to the quantification of transporter binding sites [23,24,25]. Hence, there is no technique available today that is capable to measure neuronal V_{max} *in vivo* in humans. Alternatively, well-established and easily assessable peripheral models of neuronal V_{max} such as platelet V_{max} can be utilized in humans [1,24,26,27,28]. The blood-brain relationship between platelet and neuronal 5-HTT is supported by several lines of evidence: (a) platelet and synaptosomal re-uptake are correlated in humans [26,29], (b) human blood and cerebrospinal fluid (CSF) 5-HT levels exhibit similar changes, when properly assessed [30], (c) blood and brain 5-HT levels show parallel changes after administration of 5-HT-releasing drugs [31,32], (d) platelet [33,34,35,36] and neuronal [37,38] 5-HT reuptake are heritable and genetic variation within *SLC6A4* affects 5-HT reuptake in blood cells [39,40,41,42,43,44] as well as BOLD signaling in neural circuits [45,46,47], (e) depression is associated with an increased risk of cardiovascular events putatively related to platelet dysfunction [48,49], and (f) a meta-analytical study [50] re-confirmed initial reports of an association between platelet 5-HT uptake and depression [51].

Based on above-mentioned reports on a linkage between 5-HT neurotransmission and neural activation [8,9,10,11,12,13,14,15] as well as on the correlative nature between platelet and synaptosomal V_{max} [26,29], we initiated an fMRI study in healthy subjects with the goal to investigate the putative predictive value of platelet V_{max} with respect to brain activation. Since prior studies found genetic variants within *SLC6A4* to affect 5-HTT expression [24], platelet V_{max} [41,42], and neural activation [45,46,47], genetic effects have been controlled for within this study. We expected from this novel approach to gain insights how 5-HTT function is related to neural activation in brain networks of healthy subjects.

Materials and Methods

Subjects

Right-handed healthy native speakers of European ancestry aged between 18 and 45 years were invited to participate in this study. All subjects underwent the Structured Clinical Interview for DSM-IV Axis I disorders (SCID-I) [52] to ascertain absence of any past or present psychiatric diagnoses. Moreover, subjects had to score below eight on the 21-item version of the Hamilton Depression Scale (HAM-D) [53] to be included into the study. Additionally, a medical exam was performed comprising routine blood tests, urine drug screening, a physical medical and neurological exam as well as an electrocardiogram in order to assess the medical status of the participants. Only subjects without any current or previous psychiatric or medical illness were included in this study. All assessments were conducted at the Division of Biological Psychiatry at the Medical University of Vienna (MUV). Medical exams have been performed by physicians (C.S., G.P., and L.P.). Psychological assessments have been conducted by trained raters that were supervised by these psychiatrists. Forty-eight healthy subjects (mean age 25±4.6, 31 females) fulfilled above-mentioned inclusion criteria and were enrolled in this fMRI study. All procedures were explained to participants before obtaining written informed consent. This study has been approved by the local ethics committee in line with the Declaration of Helsinki.

Laboratory Assessments

5-HT Uptake Measurement. Blood samples (50 ml) were drawn between 9 and 10 a.m. Samples were collected by venipuncture (EDTA tubes, 1% wt/vol in saline), coded, and were transferred within a 30 min timeframe after venipuncture for analysis to the Institute of Pharmacology (Center of Biomolecular Medicine and Pharmacology, MUV). Platelet-rich plasma (PRP) was separated from blood cells by centrifugation (220 g, 15 min) and diluted with Krebs–Henseleit buffer (KH; 6.92 g NaCl, 0.35 g KCl, 0.29 g $MgSO_4.7H_2O$, 0.16 g KH_2PO_4, 2.1 g $NaHCO_3$, 2.1 g glucose per liter, pH = 7.4). Briefly, platelet solution (40 µl) was incubated for three minutes with various 5-HT (0.03, 0.1, 0.3, 1.3, 10 µM unlabeled and [3H]5-HT [54]; specific activity 21.5–25.8 Ci/mmol; constant (0.03 µM), 500 µl KH). Nonspecific uptake was determined at 10 µM 5-HT in the presence of 1 µM paroxetine. Uptake was assessed by using a dilution technique with unlabeled 5-HT to reveal V_{max} and Km values (by recalculating and fitting the background-corrected uptake data to Michaelis-Menten kinetics, with c.p.m. values at the highest [5-HT] being 3–9 times over background). Uptake reactions were stopped by addition of 1 ml ice-cold KH and immediate centrifugation (41C, Sorvall-GLC-3, 1470 g). All experiments were done in triplicate determination.

Genotyping. DNA of subjects (n = 48) participating in our MRI study was isolated from EDTA blood samples using the Magna Pure LC DNA Isolation Kit (Roche). Detection of 5-HTTLPR and rs25531 were performed according to a procedure outlined elsewhere [55]. Briefly, DNA samples were subjected to polymerase chain reaction (PCR) using the primer pair 5′-TCCTCCGCTTTGGCGCCTCTTCC-3′/5′TGGGGGTTGC-AGGGGAGATCCTG-3′ to amplify long/short promoter (L/S) DNA fragments. PCR products were separated on 5% Criterion Gels (Biorad) to detect long and short promoter alleles. Part of the PCR reaction was digested by HpaII (New England Biolabs)

to detect rs25531. Digestion products were separated on 2% agarose gels. Genotyping resulted in the following genotype distribution: L_A/L_A (n = 12), L_A/L_G (n = 4), L_A/S_A (n = 20), L_A/S_G (n = 1), L_G/S_A (n = 6), S_A/S_A (n = 5). Genotypes were collapsed into a high expressing (L_A/L_A) (n = 12) and the remaining low expressing (S or L_G allele carriers) (n = 36) group for further statistical analysis [56].

Imaging Procedures

Magnetic resonance imaging. MRI measurements were performed on a 3 Tesla (3T) TIM Trio scanner and a Siemens 12-channel head coil (Siemens Medical Solutions, Erlangen, Germany). Head movements were restricted using foam pillows. Functional data were acquired via a phase corrected blipped gradient echo, single shot echo planar imaging sequence (TE/TR = 42/2000 ms, 96×96 matrix, 210 mm square FOV, 20 axial slices, slice thickness = 4 mm, slice gap = 1 mm, interleaved slice acquisition).

Paradigm. A previously published fMRI paradigm was used [46,57] that consists of two tasks comprising unpleasant emotional stimuli and one control task. Within the emotional tasks subjects had to match either one of two simultaneously presented fearful faces/threatening scenes with an identical target (face/scene). Scenes were selected from the International Affective Picture System (IAPS) [58], whereas faces were taken from the Ekman and Friesen data collection [59]. The control task consisted of simple geometric shapes that were matched analogously. The paradigm consisted of four blocks of scenes and four blocks of faces interleaved with nine blocks of the control task, 30 seconds each preceded by two seconds of instructions. Emotional tasks were grouped in blocks of two. Stimulus duration was five seconds. The total duration was 9.2 minutes. Stimuli were displayed using Presentation 10.3 (http://www.neurobs.com) and were projected onto a back-projection screen by a beamer placed outside the scanner room. Our contrast of interest was the weighted difference between affective pictures (faces and IAPS) versus the control condition (geometric shapes).

Preprocessing and Statistical Analysis

Correlation of platelet V_{max} with local activations. Preprocessing of structural and functional MRI data was performed using standard AFNI procedures (http://afni.nimh.nih.gov/afni) [60] implemented into an R framework (http://cran-r-project.or/) [61]. Briefly, preprocessing included despiking, motion correction, alignment of the functional data to the respective anatomical dataset including template alignment (TT_N27 Talairach template), spatial filtering (Gaussian kernel, 8 mm FWHM), conversion to percent signal change, and temporal filtering (frequency band 0.009–0.1 Hz). The first five volumes were discarded to ensure that magnetization equilibrium was reached. First-level whole-brain analysis was performed within a general linear model. Movement covariates and baseline drifts were modeled as regressors of no interest. The resulting contrast estimates and their respective t-statistics were then used as input for mixed-effects multilevel analysis (MEMA) to assess correlations of BOLD activation with platelet V_{max}, while controlling for age, gender, and triallelic 5-HTTLPR genotypes [62]. This approach is comparable to the conventional second level approach under conditions of normality and homogeneous effect reliability, and is superior otherwise by accounting for outliers and taking into account the reliability of effect estimates [62]. Monte Carlo simulation (10,000 iterations, dimensions: 74×87×69 grid, 2.19×2.19×2.19 mm, 9.8×9.9×9.8 mm smoothness estimated with 3dFWHMx) indicated that an initial voxel-wise threshold of $p<0.005$ and a minimum cluster size of 132 voxels yielded a corrected p value of 0.05. Additionally, we calculated cluster thresholds for more rigorous significance levels in order to indicate the statistical reproducibility of our results as recently recommended [63]. Required cluster sizes for multiple comparison correction at these more stringent thresholds were estimated to be at least 197 voxels for significant ($p<0.005$) and 245 voxels for highly significant results ($p<0.001$).

Confidence limits for the largest correlating clusters were estimated by bootstrap resampling, which avoids parametric assumptions about the distributions of the variables [64]. We further applied Cohen's f^2 in order to estimate the potential effect size of V_{max} on BOLD activity within the two most significant clusters, while controlling for age, gender, and triallelic 5-HTTLPR genotypes [65]. For these calculations, the BOLD signal was averaged across all voxels of the cluster to alleviate the effect overestimation bias that results from peak voxel selection [66].

Correlation of platelet V_{max} with functional connectivity measures. To assess the potential impact of platelet V_{max} on coherent functional networks, we calculated functional connectivity, which provides a robust measure to assess temporal correlations in the fMRI signal across functionally linked areas. Specifically, functional connectivity analysis explores which parts of the brain are coupled with a given "seed" region by cross-correlating the time series of the seed with all other voxels. Briefly, preprocessing of functional connectivity data consisted of despiking, motion correction, and alignment of functional data to the respective anatomical dataset including template alignment (TT_N27 Talairach template). Beyond the widely used removal of motion parameters derived from volume registration, we utilized the ANATICOR method [67] to eliminate nuisance signals estimated from eroded white matter and cerebrospinal fluid masks provided by FreeSurfer anatomical segmentation (FreeSurfer version 5.1.0 (http://surfer.nmr.mgh.harvard.edu/)) [68]. For temporal filtering, a broad frequency band (0.008–0.15 Hz) has been applied, which has previously been found to yield the highest test-retest reliability [69]. Finally, data have been blurred with a spatial Gaussian filter of 8 mm FWHM. To avoid any impact of task-related activations on connectivity estimates, correlation analysis was restricted to the control task blocks [70]. The selection of seeds was based on the whole-brain correlation analysis with platelet V_{max} including the largest positively and negatively correlated clusters as seeds for extraction of mean time series located in the medial prefrontal cortex (555 voxels, z = 3.756) and motor cortex (242 voxels, z = 6.942). Within first level analysis mean time series were regressed against the time series of the remaining voxels. The resulting single subject statistical seed to voxel correlation maps were then converted to z-scores using Fisher's transformation formula. Single subject z-score maps were included in a second level voxel-wise regression analysis to test for possible correlation with platelet V_{max} while controlling for age, gender, and 5-HTTLPR genotype. Monte Carlo simulation (10,000 iterations, dimensions: 74×87×69 grid, 2.19×2.19×2.19 mm, 11.0×11.3×11.5 mm smoothness) indicated that an initial voxel-wise threshold of $p<0.005$ and a minimum cluster size of 182 voxels yielded a corrected p-value of 0.05.

To further test for the impact of platelet V_{max} on pairwise connectivity between hubs of the correlating network, seeds were defined based on our correlation analysis with platelet V_{max} in core regions of the default mode network (DMN) [71] comprising the medial prefrontal cortex (mPFC), the posterior cingulate cortex (PCC), the middle temporal gyrus as well as the temporal parietal junction. To ensure equally sized seeds, each region was defined as

the 50 most significant voxels surrounding correlation peaks between V_{max} and BOLD activation. Preprocessing and second level analysis of pairwise connectivity were identical to the procedure described above. False discovery rate (FDR, $q < 0.05$) was used for multiple comparison correction of the resulting connectivity matrix.

Results

Characteristics of Platelet V_{max}

Mean platelet V_{max} of all investigated subjects was 0.124 ± 0.087 pmol/10^6 platelets/min (Table S1). Platelet V_{max} data were neither affected by age ($t_{(46)} = -0.6482$, $p = 0.5201$) nor gender ($t_{(36.72)} = -0.2081$, $p = 0.8363$). A comparison of platelet V_{max} between low (S, L_G) and high (L_A) expressing variants based on the triallelic classification of 5-HTTLPR and rs25531 resulted in a borderline significant ($t_{(15.29)} = 1.8632$, $p = 0.0488$, one-tailed) lower platelet V_{max} in S and L_G allele carriers compared to subjects with L_A/L_A genotype in line with previous results [41,42].

Correlation Analysis between Local Neural Activation and Platelet V_{max}

To investigate the potential predictive value of platelet V_{max} with respect to task-related neural activation (Text S1 and Figure S1), a voxel-wise regression analysis between platelet V_{max} and whole-brain BOLD signaling controlled for age, gender, and 5-HTTLPR genotype was performed. This analysis revealed activation clusters that significantly correlated negatively as well as positively with platelet V_{max}. Negatively correlated clusters comprised areas within the mPFC such as the anterior cingulate cortex (ACC) as well as the posterior cingulate cortex, precuneus, and left middle and inferior temporal gyrus (Figure 1, Figure S2, Figure S3, and Table 1). Importantly, all of these regions are neural nodes of the well-characterized DMN, which is suppressed during task performance and active during rest [71,72,73]. A positively correlated cluster encompassed the right motor and premotor cortex (Figure 1, Figure S2, Figure S3, and Table 1).

Bootstrap estimation of the two peak clusters exhibiting opposite correlations revealed a Pearson correlation coefficient of -0.55 (bias = 0.01; std. error = 0.12; 95% confidence interval: -0.78, -0.34) for the medial prefrontal cortex cluster (Figure S4) and 0.63 (bias = 0.01; std. error = 0.09; 95% confidence interval: 0.45, 0.80) for the motor cortex cluster (Figure S5).

With respect to effect sizes of these findings, Cohen's f^2 indicated large effects for the medial prefrontal cortex (Cohen's $f^2 = 0.40$) and the motor cortex (Cohen's $f^2 = 0.58$). However, it should be noted that effect size calculations are prone to an overestimation in fMRI studies as recently pointed out [66].

Functional Connectivity Analysis

To further investigate network characteristics of above reported regions showing significant correlations with platelet V_{max}, two *post hoc* functional connectivity analyses were conducted. The first analysis utilized the cluster showing maximal negative correlation with platelet V_{max} as seed region, whereas for the second analysis the maximally positively correlated cluster was chosen. Interestingly, whole-brain functional connectivity analyses for both seeds revealed two large and spatially highly complementary neural systems (Figure 2, Figure S6, Table S2, and Table S3). Briefly, areas showing increased coupling with the mPFC comprised the posterior cingulate cortex, precuneus, middle temporal gyrus, and temporal parietal junction, all of which correspond to core regions of the DMN that were negatively correlated to platelet V_{max} in this study [71,72]. In contrast, areas showing increased coupling with the motor cortex, which was positively correlated to platelet V_{max}, have been found exclusively in brain regions that spatially correspond to the central executive (CEN) or salience (SN) network [74,75,76,77], while functional coupling with the DMN was absent.

Notably, there was no impact of platelet V_{max} on these functional connectivity measures. Additionally, we tested for the potential impact of platelet V_{max} on pairwise intrinsic connectivity of the DMN, which was not supported by our data (Figure S7). Summarizing, our results highlight that increases in platelet V_{max} predict global DMN suppression in healthy humans.

Discussion

The present study provides evidence that platelet V_{max} predicts global DMN activation in healthy subjects. Given previous reports on platelet-synaptosomal V_{max} coupling, results of this study further suggest an important role of neuronal 5-HT reuptake in DMN regulation.

A significant negative correlation between platelet V_{max} and neural activation has predominantly been found within 5-HTT-rich cortical areas in the midline of the brain [23,78] (Figure 1, Figure S2, Figure S3, Figure S8, and Table 1). Brain regions showing an inverse relationship between platelet V_{max} and neural activation comprised areas of the mPFC including the ACC as well as the PCC, precuneus, and middle as well as inferior temporal gyrus (Figure 1, Figure S2, Figure S3), all of which are known to be core regions of the DMN [71,72,73]. Notably, the largest cluster (mPFC) even survived the application of a more rigorous significance threshold ($p < 0.001$, corrected for multiple comparisons), which indicates high statistical reproducibility [63].

Briefly, the DMN consists of above-mentioned brain regions that show marked activity during rest and low activation during focused attention on the external environment [71,72,73,79]. Prevailing hypotheses conceptualize the physiological role of the DMN as primarily related to self-referential thought (e.g. internal mentation, day dreaming, etc.) [79]. A major feature of the DMN is its suppression during attention-demanding tasks. This anti-correlative suppression is necessary for proper task performance and avoids 'mind wandering' resulting from conflicting self-referential computations [79]. Lacking DMN suppression during attention-demanding tasks is of clinical importance and has been linked to increased rumination in depressed patients [80,81].

The observed coupling between platelet V_{max} and core regions of the DMN is of specific interest, because a thorough understanding of the neurochemical regulation of the DMN is still missing [20]. Available evidence indicates that monoamines such as dopamine and 5-HT play a major regulatory role [16,20,82,83,84,85]. Dopamine affects DMN coupling with attention networks [82] and the application of dopaminergic agents such as modafinil leads to DMN suppression [83]. An analogous suppression of the DMN can be achieved by serotonergic agents such as the 5-HT_{2A}/5-HT_{2C} agonist psilocybin [84]. Moreover, 5-HT_{1A} autoreceptor binding has been shown to be anti-correlated with PCC activation, while opposing effects were found for retrosplenial and medial prefrontal DMN regions [20]. A similar regionally-specific effect of serotonergic neurotransmission on DMN activity has been reported in a tryptophan depletion study [85]. Given the spatial co-occurrence between cortical regions of high 5-HTT densities and nodes of the DMN [23,78] (Text S1 and Figure S8), it is interesting that 5-HT reuptake inhibition with escitalopram or combined 5-HT and norepinephrine inhibition with duloxetine have been demonstrated to decrease DMN coupling in human phMRI studies [16,86].

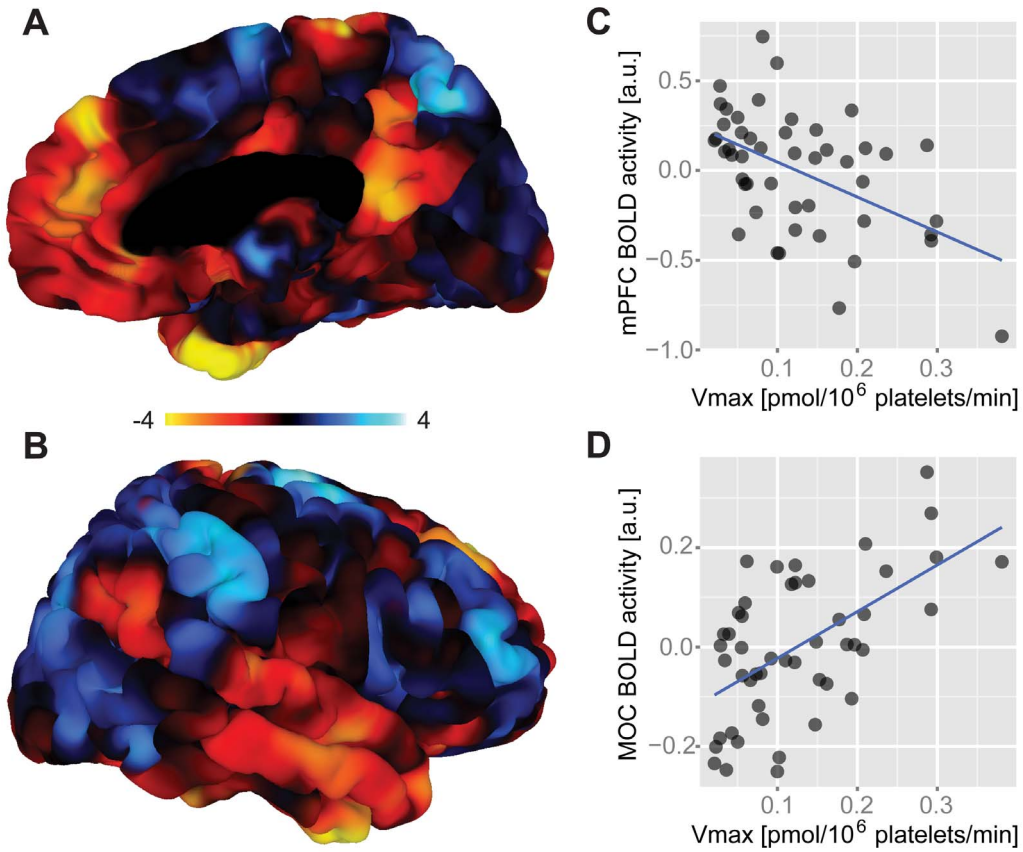

Figure 1. Functional brain correlates of platelet 5-HT uptake velocity. (**A–B**) Figures display right-hemispheric surface mappings of a whole-brain correlation analysis between platelet V_{max} and BOLD activity (n = 48). Significant brain areas showed positive and negative correlations. Negatively correlated clusters comprised areas of the DMN such as regions within the mPFC/ACC as well as the PCC, MTG, and ITG. Positive correlations were found in the fronto-parietal control system encompassing the CEN and SN with a significant cluster located in the right MOC and PMC. The corresponding left-hemispheric mapping is shown in Figure S2. Colorbar represents t-values. (**C**) Scatter plot shows the negative relationship between platelet V_{max} and BOLD activity averaged across the mPFC cluster (peak at [−7.7, 44.1, 27.5]). (**D**) Scatter plot shows the positive relationship between platelet V_{max} and BOLD activity averaged across the MOC cluster (peak at [20.8, −21.6, 69.1]). All analyses are controlled for age, gender and 5-HTTLPR. Serotonin, 5-HT; maximal 5-HT uptake velocity, V_{max}; default mode network, DMN; medial prefrontal cortex, mPFC; anterior cingulate cortex, ACC; posterior cingulate cortex, PCC; middle temporal gyrus, MTG; inferior temporal gyrus, ITG; central executive network, CEN; salience network, SN; motor cortex, MOC; premotor cortex, PMC; blood-oxygen-level dependent, BOLD; a.u., arbitrary units.
doi:10.1371/journal.pone.0092543.g001

Notably, pharmacological challenge studies [16,86] are not well suited to study the physiological effects of 5-HT reuptake on DMN activation. However, the absence of any effect would have made the existence of a physiologic coupling between 5-HT reuptake and DMN activity implausible. Hence, the studies of *Van der Ven et al.* [16] and *Van Wingen et al.* [86] together with other studies [20,84,85] clearly indicate an important role of brain 5-HT in the regulation of the DMN. Our finding of a negative correlation between platelet V_{max} and DMN activity provides further evidence for a possible impact of 5-HT transport processes in the regulation of the DMN. Moreover, the observed coupling between platelet V_{max} and neural activity indirectly supports the idea that platelet 5-HT reuptake can indeed be utilized as surrogate marker of neural 5-HT reuptake, which is in accordance with studies showing a coupling between platelet and synaptosomal 5-HT reuptake [26] as well as others that demonstrated 5-HTT-mediated effects on BOLD signaling [8,9,10,11,12,13,14,15].

While the majority of brain regions showed a negative correlation with platelet V_{max} in our study, we report a single cluster of neural activation that correlates positively with platelet V_{max} (Figure 1, Figure S3, Figure S5, and Table 1). This cluster comprises the primary motor and premotor cortex that is related to motor function or motor learning [87]. It is noteworthy that these regions are engaged during the performance of externally-oriented tasks and are therefore active, when the DMN is typically suppressed [75]. This is in line with our functional connectivity analysis of this cluster that revealed no connectivity to the DMN, but a widely distributed network of significantly coupled cortical regions belonging to the CEN and SN (Figure 2 and Figure S6). Both CEN and SN are large brain networks of the fronto-parietal control system that have intensively been investigated using resting-state and task-based fMRI [74,75,76,77]. While the CEN has been related to high-level cognitive functions such as working memory and attention control, the SN responds to behaviorally salient events and has been implicated in switching between endogenously and exogenously driven mental activity [77]. Anatomically, dorsolateral prefrontal and posterior parietal cortices have been identified as nodes of the CEN, whereas the SN is anchored in the anterior insular and dorsal anterior cingulate cortex [77].

This study further investigated the possibility that variability in platelet V_{max} might explain changes of DMN intrinsic connectivity. This question was asked, because recent studies reported a

Table 1. Correlation analysis between maximal platelet 5-HT uptake velocity (V_{max}) and neuronal activation (n = 48).

Region	Hemisphere	Size	z	p	x	y	z
mPFC, ACC	R/L	555	−3.756	<0.001***	−7.7	44.1	27.5
MOC, PMC	R	242	6.942	<0.001**	20.8	−21.6	69.1
PCC, PRE	R/L	189	−3.503	<0.001*	3.3	−47.8	14.4
MTG, ITG	L	167	−4.542	<0.001*	−55.8	−10.6	−9.7

Medial prefrontal cortex, mPFC; anterior cingulate cortex, ACC; motor cortex, MOC; premotor cortex, PMC; posterior cingulate cortex, PCC; precuneus, PRE; middle temporal gyrus, MTG; inferior temporal gyrus, ITG; p, uncorrected p value; significance level after correction for multiple comparisons based on recent recommendations [63]: ***p<0.001; **p<0.005; *p<0.05; x, y, z are coordinates in Talairach space; L, left hemisphere; R, right hemisphere; cluster size expressed as number of voxels.

doi:10.1371/journal.pone.0092543.t001

modulation of medial DMN intrinsic connectivity after pharmacological challenge with serotonergic drugs [16,84,86,88]. In contrast, our results do not support the idea that synaptic 5-HT reuptake is altering the pair-wise coupling of DMN nodes (Figure S7). Given the inconsistency of reported changes of connections in between DMN nodes [16,84,86,89], we argue that observed alterations are likely rather reflecting effects related to the specific drug being used than effects related to synaptic 5-HT reuptake in general. Moreover, the reported findings might only apply to more extreme changes of synaptic 5-HT reuptake that go along with pharmacological interventions. Hence, we are tempted to speculate that 5-HT reuptake is not affecting intrinsic DMN connectivity *in vivo* under physiologic conditions.

Previous studies reported effects of genetic variability within the 5-HTT gene (*SLC6A4*) on 5-HTT expression [90], platelet V_{max} [41,42], and BOLD signaling [45,46]. Since both platelet and neural 5-HTTs are encoded by the same gene, we investigated the potential impact of genetic variants within *SLC6A4* on platelet V_{max} and the observed correlation between platelet V_{max} and BOLD signaling. The comparison of platelet V_{max} between low (S, L_G) and high (L_A) expressing variants of 5-HTTLPR and rs25531

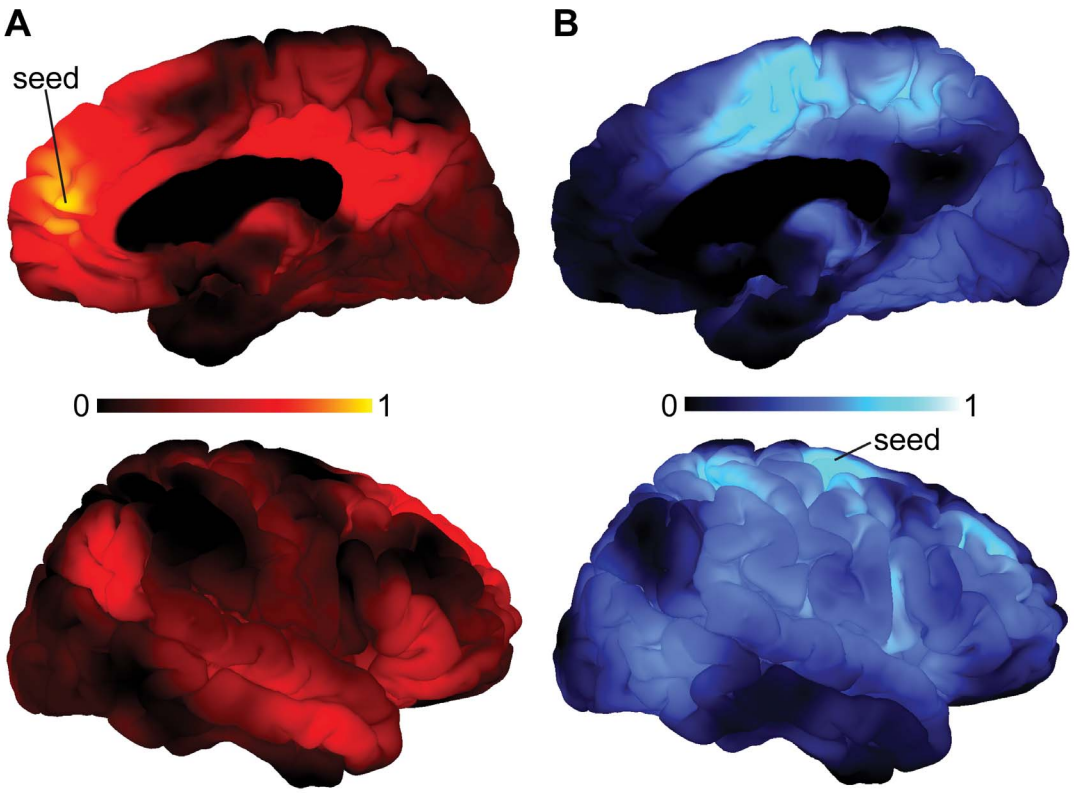

Figure 2. Functional connectivity analysis of the mPFC and MOC cluster. (**A**) Figures display right-hemispheric surface mappings of a functional connectivity analysis utilizing the mPFC cluster as seed region. Areas showing increased coupling with the mPFC comprised the PCC, precuneus, MTG and temporal parietal junction. All of these areas correspond to core regions of the DMN. (**B**) Figures display right-hemispheric surface mappings of a functional connectivity analysis utilizing the MOC cluster as seed region. Areas showing increased coupling with the MOC have been found exclusively in brain regions that spatially correspond to the CEN or SN, while functional coupling with the DMN was absent. The corresponding left-hemispheric mappings are shown in Figure S6. Colorbars represent mean Pearson's r. Medial prefrontal cortex, mPFC; posterior cingulate cortex, PCC; middle temporal gyrus, MTG; motor cortex, MOC; default-mode network, DMN; central executive network, CEN; salience network, SN.

doi:10.1371/journal.pone.0092543.g002

revealed lower platelet V_{max} in S and L_G allele carriers in comparison to subjects with L_A/L_A genotype. This finding reflects the lower transcription efficacy of the S allele [56] thereby resembling previous reports [41,42]. Importantly, we found significant correlations between V_{max} and the BOLD signal in DMN areas despite controlling for triallelic 5-HTTLPR, what suggests that this finding cannot be attributed to 5-HTTLPR or rs25531 alone. It is noteworthy, however, that stress-dependent promoter methylation of 5-HTTLPR alleles might significantly vary between platelet precursor cells and neural cells thereby underscoring epigenetic differences in blood and brain [91,92,93,94]. Hence, our finding points towards the possible importance of other biological factors affecting both, platelet and neuronal V_{max}. Possible candidates among others would be genetic variability within *SEC24* that has been demonstrated to affect the correct delivery of 5-HTTs to the cell surface [95] or cytokine signaling that impacts on 5-HTT availability in platelets and neurons [96,97].

Some precautions should be considered within the context of this study. Firstly, we assessed platelet V_{max}, which was used as surrogate marker of synaptosomal V_{max} in this study, due to the fact that synaptosomal V_{max} cannot be measured *in vivo* in humans [1,24,26,27]. The rationale for using platelet V_{max} as estimator of synaptosomal V_{max} is further based on studies that reported a coupling between platelet and synaptosomal V_{max} [26,29] as well as blood and CSF 5-HT levels with [31,32] or without [30] 5-HT challenge. Moreover, platelet and synaptosomal V_{max} are heritable [33,34,35,36] and genetic variation within *SLC6A4* affects 5-HT reuptake in platelets [39,40,41,42,43,44] as well as neural signaling [45,46]. Secondly, conclusions drawn within this investigation are derived from findings of phMRI studies that reported tight associations between 5-HT neurotransmission and BOLD signaling in humans [10,11,12,13,14,15,16] and animals [8,9]. Since both *a priori* assumptions (platelet and synaptosomal V_{max} coupling as well as measurable effects of 5-HT reuptake on BOLD signaling) are founded on multiple scientific reports conducted in the past, we are confident that our conclusions are not too far-fetched. However, replication studies are needed before final conclusions with respect to the reported association between platelet V_{max} and DMN activation can be drawn. Another interesting question is why the subgenual cingulate cortex (sACC) [98,99], which shows the highest cortical 5-HTT binding in *post mortem* studies [78] and in own PET data (Figure S9, Text S1, and Table S4), has not been found to be the main peak of correlation with platelet V_{max} within this study given its repeated implication in depression neurobiology [98] and therapy [99]. Aside from the fact that the sACC was actually part of the medial prefrontal cluster that correlated significantly with platelet $V_{max,}$ it is noteworthy to highlight that this region is located in a part of the brain that is prone to high data variance due to susceptibility artifacts. This has likely led to a disadvantageous signal-to-noise ratio in this region and a higher chance to statistically fail in a whole-brain analysis. Hence, replication studies with larger sample size are clearly needed to re-evaluate the specific role of the sACC in this context.

Summarizing, we found that platelet V_{max} is predicting global DMN activity in healthy humans *in vivo*. Considering previous studies that have demonstrated a tight coupling between platelet and synaptosomal V_{max}, this study suggests an important role of neuronal 5-HT reuptake in DMN regulation. The feasibility to use a blood measure to predict a well-characterized neural pattern, as shown in this study, encourages ongoing studies investigating putative blood biomarkers of neural phenotypes.

Supporting Information

Figure S1 Task activation. Brain activation during processing of emotional pictures (faces+IAPS), contrasted against processing of neutral pictures (geometric shapes). Data is displayed at $p<0.005$. Colorbar represents z-scores.
(PDF)

Figure S2 Functional brain correlates of platelet 5-HT uptake velocity. Figures display left-hemispheric surface mappings of a whole-brain correlation analysis between platelet V_{max} and BOLD activity ($n = 48$). Significant brain areas showed positive and negative correlations. Negatively correlated clusters comprised areas of the DMN such as regions within the mPFC/ACC as well as the PCC, MTG, and ITG. Positive correlations were found in the fronto-parietal control system encompassing the CEN and SN. The corresponding right-hemispheric mapping is shown in Figure 1. Colorbar represents t-values. All analyses are controlled for age, gender and 5-HTTLPR. Serotonin, 5-HT; maximal 5-HT uptake velocity, V_{max}; medial prefrontal cortex, mPFC; anterior cingulate cortex, ACC; posterior cingulate cortex, PCC; middle temporal gyrus, MTG; inferior temporal gyrus, ITG; motor cortex, MOC; premotor cortex, PMC; default-mode network, DMN; central executive network, CEN; salience network, SN.
(PDF)

Figure S3 Functional brain correlates of platelet 5-HT uptake velocity. Figures display a whole-brain correlation analysis between platelet V_{max} and BOLD activity ($n = 48$) corrected for age, gender, and 5-HTTLPR genotype (threshold $p<0.005$, colorbar represents t-values). Significant brain areas showed positive and negative correlations. Negatively correlated clusters comprised areas of the DMN such as regions within the mPFC including the ACC as well as the PCC, MTG, and ITG. Positive correlations were found in the fronto-parietal control system encompassing the CEN and SN with a significant cluster located in the right MOC and PMC. The corresponding surface mappings are shown in Figure 1 and Figure S2. Serotonin, 5-HT; maximal 5-HT uptake velocity, Vmax; medial prefrontal cortex, mPFC; anterior cingulate cortex, ACC; posterior cingulate cortex, PCC; middle temporal gyrus, MTG; inferior temporal gyrus, ITG; motor cortex, MOC; premotor cortex, PMC; default-mode network, DMN; central executive network, CEN; salience network, SN.
(PDF)

Figure S4 Bootstrap distribution of the correlation between the BOLD signal in the medial prefrontal cortex (mPFC) cluster and platelet serotonin uptake velocity (V_{max}). The original statistic is indicated in red.
(PDF)

Figure S5 Bootstrap distribution of the correlation between the BOLD signal in the motor cortex (MOC) cluster and platelet serotonin uptake velocity (V_{max}). The original statistic is indicated in red.
(PDF)

Figure S6 Functional connectivity analysis of the mPFC and MOC cluster. **(A)** Figures display left-hemispheric surface mappings of a functional connectivity analysis utilizing the mPFC cluster as seed region. Areas showing increased coupling with the mPFC comprised the PCC, precuneus, MTG and temporal parietal junction. All of these areas correspond to core regions of the DMN. **(B)** Figures display left-hemispheric surface mappings of a functional connectivity analysis utilizing the MOC cluster as

seed region. Since this seed is located in the right hemisphere, it is not depicted in the figure. Areas showing increased coupling with the MOC have been found exclusively in brain regions that spatially correspond to the CEN or SN, while functional coupling with the DMN was absent. The corresponding right-hemispheric mappings are shown in Figure 2. Colorbars represent mean Pearson's r. Medial prefrontal cortex, mPFC; posterior cingulate cortex, PCC; middle temporal gyrus, MTG; motor cortex, MOC; default-mode network, DMN; central executive network, CEN; salience network, SN.
(PDF)

Figure S7 Correlation of platelet V_{max} and intrinsic connectivity of the DMN. The connectivity matrix displays z-scores of the correlation between platelet serotonin uptake velocity (V_{max}) and the intrinsic connectivity of the default mode network (DMN). There was no significant correlation between platelet V_{max} and intrinsic connectivity of the DMN. False discovery rate (FDR) was used for multiple comparison correction ($q < 0.5$). Medial prefrontal cortex, mPFC; posterior cingulate cortex, PCC; right middle temporal gyrus, r MTG; left middle temporal gyrus, l MTG; left temporal parietal junction, l TPJ; right temporal parietal junction, r TPJ.
(PDF)

Figure S8 Cortical expression map of *SLC6A4* of all available adults of European ancestry within the Allen Human Brain Atlas collection. Illustrated are ranked and averaged z-scores for cortical regions. Zero on the Y-axis refers to average cortical expression in the brain. Please note that all DMN regions are exhibiting increased expression values.
(PDF)

Figure S9 Surface mapping displays regional areas of increased serotonin transporter (5-HTT) availability within the cingulate cortex (CC) in healthy subjects (n = 8). [11C]DASB PET data have been tested against deviation from mean CC binding. It is noteworthy that the subgenual anterior cingulate cortex (sACC) contains the largest cluster of significant voxels within the whole CC. Colorbar represents t-values.
(PDF)

Table S1 Differences in maximal platelet serotonin (5-HT) uptake velocity (V_{max}, in pmol/10^6 platelets/min) and age between male and female subjects. n – number of subjects. std – standard deviation.
(DOC)

Table S2 Regions exhibiting maximal connectivity to the medial prefrontal cortex cluster, thresholded at Pearson's r >0.5. [a]Pearson's r. [b]Coordinates are given in Talairach space.
(DOC)

Table S3 Regions exhibiting maximal connectivity to the motor cortex cluster, thresholded at Pearson's r >0.5. [a]Pearson's r. [b]Coordinates are given in Talairach space.
(DOC)

Table S4 Clusters of locally significantly increased serotonin transporter (5-HTT) availability compared to the whole cingulate cortex (CC). [a]Uncorrected z-scores next to corresponding FWE-corrected one-tailed p values. [b]Coordinates are given in Talairach space.
(DOC)

Text S1 Supplementary methods.
(DOC)

Acknowledgments

We thank V. Köller, H. Oswald, N. Schwidde, and D. Mandorfer for their assistance in subject recruitment and evaluation, K. Kohler and S. Walther for their assistance in performing 5-HT uptake experiments, L. Klingler for his help in genetic analysis, and W. Wadsak, M. Mitterhauser, and M. Savli for PET radiosyntheses and PET data processing. We are thankful to S. Russo-Schwarzbaum for preparation of experiments and piloting data analysis. Furthermore, we are indebted to A. Berger for providing technical support and to A. Popovic for her help in recruitment and clinical evaluation. Finally, we thank A. Holmes and D.R. Weinberger for critical comments on our manuscript.

Author Contributions

Conceived and designed the experiments: HE BB EM HHS LP MW MF AML. Performed the experiments: CS UR CHK TH LB GP ZU BH. Analyzed the data: UR CHK BMM KD HHS KK. Contributed reagents/materials/analysis tools: WH KK TP HH AML SK CW RL HE EM HHS LP. Wrote the paper: CS UR CHK BMM KD LB WH TP HH AML SK MF CW MW RL EH BB EM HHS LP.

References

1. Mercado CP, Kilic F (2010) Molecular mechanisms of SERT in platelets: regulation of plasma serotonin levels. Mol Interv 10: 231–241.
2. Cools R, Roberts AC, Robbins TW (2008) Serotoninergic regulation of emotional and behavioural control processes. Trends Cogn Sci 12: 31–40.
3. Krishnan V, Nestler EJ (2008) The molecular neurobiology of depression. Nature 455: 894–902.
4. Kupfer DJ, Frank E, Phillips ML (2012) Major depressive disorder: new clinical, neurobiological, and treatment perspectives. Lancet 379: 1045–1055.
5. Bauer M, Pfennig A, Severus E, Whybrow PC, Angst J, et al. (2013) World Federation of Societies of Biological Psychiatry (WFSBP) guidelines for biological treatment of unipolar depressive disorders, part 1: update 2013 on the acute and continuation treatment of unipolar depressive disorders. World J Biol Psychiatry 14: 334–385.
6. Hyman SE (2008) A glimmer of light for neuropsychiatric disorders. Nature 455: 890–893.
7. Graham J, Salimi-Khorshidi G, Hagan C, Walsh N, Goodyer I, et al. (2013) Meta-analytic evidence for neuroimaging models of depression: state or trait? J Affect Disord 151: 423–431.
8. Klomp A, Tremoleda JL, Schrantee A, Gsell W, Reneman L (2012) The use of pharmacological-challenge fMRI in pre-clinical research: application to the 5-HT system. J Vis Exp.
9. Preece MA, Taylor MJ, Raley J, Blamire A, Sharp T, et al. (2009) Evidence that increased 5-HT release evokes region-specific effects on blood-oxygenation level-dependent functional magnetic resonance imaging responses in the rat brain. Neuroscience 159: 751–759.
10. McKie S, Del-Ben C, Elliott R, Williams S, del Vai N, et al. (2005) Neuronal effects of acute citalopram detected by pharmacoMRI. Psychopharmacology (Berl) 180: 680–686.
11. Bigos KL, Pollock BG, Aizenstein HJ, Fisher PM, Bies RR, et al. (2008) Acute 5-HT reuptake blockade potentiates human amygdala reactivity. Neuropsychopharmacology 33: 3221–3225.
12. Windischberger C, Lanzenberger R, Holik A, Spindelegger C, Stein P, et al. (2010) Area-specific modulation of neural activation comparing escitalopram and citalopram revealed by pharmaco-fMRI: a randomized cross-over study. Neuroimage 49: 1161–1170.
13. Anderson IM, Juhasz G, Thomas E, Downey D, McKie S, et al. (2011) The effect of acute citalopram on face emotion processing in remitted depression: a pharmacoMRI study. Eur Neuropsychopharmacol 21: 140–148.
14. Sheline YI, Barch DM, Donnelly JM, Ollinger JM, Snyder AZ, et al. (2001) Increased amygdala response to masked emotional faces in depressed subjects resolves with antidepressant treatment: an fMRI study. Biol Psychiatry 50: 651–658.
15. Fu CH, Williams SC, Cleare AJ, Brammer MJ, Walsh ND, et al. (2004) Attenuation of the neural response to sad faces in major depression by antidepressant treatment: a prospective, event-related functional magnetic resonance imaging study. Arch Gen Psychiatry 61: 877–889.

16. van de Ven V, Wingen M, Kuypers KP, Ramaekers JG, Formisano E (2013) Escitalopram Decreases Cross-Regional Functional Connectivity within the Default-Mode Network. PLoS One 8: e68355.
17. Hoflich A, Baldinger P, Savli M, Lanzenberger R, Kasper S (2012) Imaging treatment effects in depression. Rev Neurosci 23: 227–252.
18. Neumeister A, Nugent AC, Waldeck T, Geraci M, Schwarz M, et al. (2004) Neural and behavioral responses to tryptophan depletion in unmedicated patients with remitted major depressive disorder and controls. Arch Gen Psychiatry 61: 765–773.
19. Passamonti L, Crockett MJ, Apergis-Schoute AM, Clark L, Rowe JB, et al. (2012) Effects of acute tryptophan depletion on prefrontal-amygdala connectivity while viewing facial signals of aggression. Biol Psychiatry 71: 36–43.
20. Hahn A, Wadsak W, Windischberger C, Baldinger P, Hoflich AS, et al. (2012) Differential modulation of the default mode network via serotonin-1A receptors. Proc Natl Acad Sci U S A 109: 2619–2624.
21. Fisher PM, Meltzer CC, Price JC, Coleman RL, Ziolko SK, et al. (2009) Medial prefrontal cortex 5-HT(2A) density is correlated with amygdala reactivity, response habituation, and functional coupling. Cereb Cortex 19: 2499–2507.
22. Rhodes RA, Murthy NV, Dresner MA, Selvaraj S, Stavrakakis N, et al. (2007) Human 5-HT transporter availability predicts amygdala reactivity in vivo. J Neurosci 27: 9233–9237.
23. Savli M, Bauer A, Mitterhauser M, Ding YS, Hahn A, et al. (2012) Normative database of the serotonergic system in healthy subjects using multi-tracer PET. Neuroimage 63: 447–459.
24. Willeit M, Sitte HH, Thierry N, Michalek K, Praschak-Rieder N, et al. (2008) Enhanced serotonin transporter function during depression in seasonal affective disorder. Neuropsychopharmacology 33: 1503–1513.
25. Baldinger P, Kranz GS, Haeusler D, Savli M, Spies M, et al. (2013) Regional differences in SERT occupancy after acute and prolonged SSRI intake investigated by brain PET. Neuroimage.
26. Rausch JL, Johnson ME, Li J, Hutcheson J, Carr BM, et al. (2005) Serotonin transport kinetics correlated between human platelets and brain synaptosomes. Psychopharmacology (Berl) 180: 391–398.
27. Yubero-Lahoz S, Robledo P, Farre M, de laTorre R (2013) Platelet SERT as a peripheral biomarker of serotonergic neurotransmission in the central nervous system. Curr Med Chem 20: 1382–1396.
28. Hayashi-Takagi A, Vawter MP, Iwamoto K (2013) Peripheral Biomarkers Revisited: Integrative Profiling of Peripheral Samples for Psychiatric Research. Biol Psychiatry.
29. Uebelhack R, Franke L, Herold N, Plotkin M, Amthauer H, et al. (2006) Brain and platelet serotonin transporter in humans-correlation between [123I]-ADAM SPECT and serotonergic measurements in platelets. Neurosci Lett 406: 153–158.
30. Audhya T, Adams JB, Johansen L (2012) Correlation of serotonin levels in CSF, platelets, plasma, and urine. Biochim Biophys Acta 1820: 1496–1501.
31. Collins CM, Kloek J, Elliott JM (2012) Parallel changes in serotonin levels in brain and blood following acute administration of MDMA. J Psychopharmacol.
32. Yubero-Lahoz S, Ayestas MA, Jr., Blough BE, Partilla JS, Rothman RB, et al. (2012) Effects of MDMA and related analogs on plasma 5-HT: relevance to 5-HT transporters in blood and brain. Eur J Pharmacol 674: 337–344.
33. Meltzer HY, Arora RC (1988) Genetic control of serotonin uptake in blood platelets: a twin study. Psychiatry Res 24: 263–269.
34. Abney M, McPeek MS, Ober C (2001) Broad and narrow heritabilities of quantitative traits in a founder population. Am J Hum Genet 68: 1302–1307.
35. Anderson GM, Czarkowski K, Ravski N, Epperson CN (2004) Platelet serotonin in newborns and infants: ontogeny, heritability, and effect of in utero exposure to selective serotonin reuptake inhibitors. Pediatr Res 56: 418–422.
36. Jernej B, Cicin-Sain L (1990) Platelet serotonin level in rats is under genetic control. Psychiatry Res 32: 167–174.
37. Frokjaer VG, Vinberg M, Erritzoe D, Svarer C, Baare W, et al. (2009) High familial risk for mood disorder is associated with low dorsolateral prefrontal cortex serotonin transporter binding. Neuroimage 46: 360–366.
38. Steiger H, Gauvin L, Joober R, Israel M, Ng Ying Kin NM, et al. (2006) Intrafamilial correspondences on platelet [3H-]paroxetine-binding indices in bulimic probands and their unaffected first-degree relatives. Neuropsychopharmacology 31: 1785–1792.
39. Anderson GM, Gutknecht L, Cohen DJ, Brailly-Tabard S, Cohen JH, et al. (2002) Serotonin transporter promoter variants in autism: functional effects and relationship to platelet hyperserotonemia. Mol Psychiatry 7: 831–836.
40. Lesch KP, Bengel D, Heils A, Sabol SZ, Greenberg BD, et al. (1996) Association of anxiety-related traits with a polymorphism in the serotonin transporter gene regulatory region. Science 274: 1527–1531.
41. Greenberg BD, Tolliver TJ, Huang SJ, Li Q, Bengel D, et al. (1999) Genetic variation in the serotonin transporter promoter region affects serotonin uptake in human blood platelets. Am J Med Genet 88: 83–87.
42. Nobile M, Begni B, Giorda R, Frigerio A, Marino C, et al. (1999) Effects of serotonin transporter promoter genotype on platelet serotonin transporter functionality in depressed children and adolescents. J Am Acad Child Adolesc Psychiatry 38: 1396–1402.
43. Singh YS, Altieri SC, Gilman TL, Michael HM, Tomlinson ID, et al. (2012) Differential serotonin transport is linked to the rh5-HTTLPR in peripheral blood cells. Transl Psychiatry 2: e77.
44. Singh YS, Sawarynski LE, Michael HM, Ferrell RE, Murphey-Corb MA, et al. (2010) Boron-Doped Diamond Microelectrodes Reveal Reduced Serotonin Uptake Rates in Lymphocytes from Adult Rhesus Monkeys Carrying the Short Allele of the 5-HTTLPR. ACS Chem Neurosci 1: 49–64.
45. Pezawas L, Meyer-Lindenberg A, Drabant EM, Verchinski BA, Munoz KE, et al. (2005) 5-HTTLPR polymorphism impacts human cingulate-amygdala interactions: a genetic susceptibility mechanism for depression. Nat Neurosci 8: 828–834.
46. Hariri AR, Mattay VS, Tessitore A, Kolachana B, Fera F, et al. (2002) Serotonin transporter genetic variation and the response of the human amygdala. Science 297: 400–403.
47. Scharinger C, Rabl U, Pezawas L, Kasper S (2011) The genetic blueprint of major depressive disorder: contributions of imaging genetics studies. World J Biol Psychiatry 12: 474–488.
48. Baune BT, Stuart M, Gilmour A, Wersching H, Heindel W, et al. (2012) The relationship between subtypes of depression and cardiovascular disease: a systematic review of biological models. Transl Psychiatry 2: e92.
49. Ziegelstein RC, Parakh K, Sakhuja A, Bhat U (2009) Platelet function in patients with major depression. Intern Med J 39: 38–43.
50. Ellis PM, Salmond C (1994) Is platelet imipramine binding reduced in depression? A meta-analysis. Biol Psychiatry 36: 292–299.
51. Meltzer HY, Arora RC, Baber R, Tricou BJ (1981) Serotonin uptake in blood platelets of psychiatric patients. Arch Gen Psychiatry 38: 1322–1326.
52. APA (2000) Diagnostic and statistical manual of mental disorders: DSM-IV-TR. Washington, DC: American Psychiatric Association.
53. Hamilton M (1960) A rating scale for depression. J Neurol Neurosurg Psychiatry 23: 56–62.
54. Scholze P, Sitte HH, Singer EA (2001) Substantial loss of substrate by diffusion during uptake in HEK-293 cells expressing neurotransmitter transporters. Neurosci Lett 309: 173–176.
55. Wendland JR, Martin BJ, Kruse MR, Lesch KP, Murphy DL (2006) Simultaneous genotyping of four functional loci of human SLC6A4, with a reappraisal of 5-HTTLPR and rs25531. Mol Psychiatry 11: 224–226.
56. Hu XZ, Lipsky RH, Zhu G, Akhtar LA, Taubman J, et al. (2006) Serotonin transporter promoter gain-of-function genotypes are linked to obsessive-compulsive disorder. Am J Hum Genet 78: 815–826.
57. Kirsch P, Esslinger C, Chen Q, Mier D, Lis S, et al. (2005) Oxytocin modulates neural circuitry for social cognition and fear in humans. J Neurosci 25: 11489–11493.
58. Lang PJ, Bradley MM, Cuthbert BN (1997) International affective picture system (IAPS). Technical manual and affective ratings. Technical report, NIMH Center for the Study of Emotion and Attention, University of Florida, Gainesville.
59. Ekman P, Friesen W (1978) Facial action coding system: A technique for the measurement of facial movement. Palo Alto, Calif.: Consulting Psychologists Press.
60. Cox RW (1996) AFNI: software for analysis and visualization of functional magnetic resonance neuroimages. Comput Biomed Res 29: 162–173.
61. Boubela RN, Huf W, Kalcher K, Sladky R, Filzmoser P, et al. (2012) A highly parallelized framework for computationally intensive MR data analysis. MAGMA 25: 313–320.
62. Chen G, Saad ZS, Nath AR, Beauchamp MS, Cox RW (2012) FMRI group analysis combining effect estimates and their variances. Neuroimage 60: 747–765.
63. Johnson VE (2013) Revised standards for statistical evidence. Proc Natl Acad Sci U S A 110: 19313–19317.
64. Efron B, Tibshirani R (1993) An Introduction to the Bootstrap: Chapman and Hall.
65. Cohen JE, editor (1988) Statistical Power Analysis for the Behavioral Sciences. Hillsdale, NY: Lawrence Erlbaum Associates, Inc.
66. Vul E, Pashler H (2012) Voodoo and circularity errors. Neuroimage 62: 945–948.
67. Jo HJ, Saad ZS, Simmons WK, Milbury LA, Cox RW (2010) Mapping sources of correlation in resting state FMRI, with artifact detection and removal. Neuroimage 52: 571–582.
68. Fischl B, Salat DH, Busa E, Albert M, Dieterich M, et al. (2002) Whole brain segmentation: automated labeling of neuroanatomical structures in the human brain. Neuron 33: 341–355.
69. Braun U, Plichta MM, Esslinger C, Sauer C, Haddad L, et al. (2012) Test-retest reliability of resting-state connectivity network characteristics using fMRI and graph theoretical measures. Neuroimage 59: 1404–1412.
70. Fair DA, Schlaggar BL, Cohen AL, Miezin FM, Dosenbach NU, et al. (2007) A method for using blocked and event-related fMRI data to study "resting state" functional connectivity. Neuroimage 35: 396–405.
71. Buckner RL, Andrews-Hanna JR, Schacter DL (2008) The brain's default network: anatomy, function, and relevance to disease. Ann N Y Acad Sci 1124: 1–38.
72. Greicius MD, Krasnow B, Reiss AL, Menon V (2003) Functional connectivity in the resting brain: a network analysis of the default mode hypothesis. Proc Natl Acad Sci U S A 100: 253–258.
73. Raichle ME, MacLeod AM, Snyder AZ, Powers WJ, Gusnard DA, et al. (2001) A default mode of brain function. Proceedings of the National Academy of Sciences of the United States of America 98: 676–682.
74. Seeley WW, Menon V, Schatzberg AF, Keller J, Glover GH, et al. (2007) Dissociable intrinsic connectivity networks for salience processing and executive control. J Neurosci 27: 2349–2356.

75. Fox MD, Snyder AZ, Vincent JL, Corbetta M, Van Essen DC, et al. (2005) The human brain is intrinsically organized into dynamic, anticorrelated functional networks. Proc Natl Acad Sci U S A 102: 9673–9678.
76. Menon V (2011) Large-scale brain networks and psychopathology: a unifying triple network model. Trends Cogn Sci 15: 483–506.
77. Bressler SL, Menon V (2010) Large-scale brain networks in cognition: emerging methods and principles. Trends Cogn Sci 14: 277–290.
78. Varnas K, Halldin C, Hall H (2004) Autoradiographic distribution of serotonin transporters and receptor subtypes in human brain. Hum Brain Mapp 22: 246–260.
79. Anticevic A, Cole MW, Murray JD, Corlett PR, Wang XJ, et al. (2012) The role of default network deactivation in cognition and disease. Trends Cogn Sci 16: 584–592.
80. Sheline YI, Barch DM, Price JL, Rundle MM, Vaishnavi SN, et al. (2009) The default mode network and self-referential processes in depression. Proc Natl Acad Sci U S A 106: 1942–1947.
81. Hamilton JP, Furman DJ, Chang C, Thomason ME, Dennis E, et al. (2011) Default-mode and task-positive network activity in major depressive disorder: implications for adaptive and maladaptive rumination. Biol Psychiatry 70: 327–333.
82. Dang LC, O'Neil JP, Jagust WJ (2012) Dopamine supports coupling of attention-related networks. J Neurosci 32: 9582–9587.
83. Minzenberg MJ, Yoon JH, Carter CS (2011) Modafinil modulation of the default mode network. Psychopharmacology (Berl) 215: 23–31.
84. Carhart-Harris RL, Erritzoe D, Williams T, Stone JM, Reed LJ, et al. (2012) Neural correlates of the psychedelic state as determined by fMRI studies with psilocybin. Proc Natl Acad Sci U S A 109: 2138–2143.
85. Kunisato Y, Okamoto Y, Okada G, Aoyama S, Demoto Y, et al. (2011) Modulation of default-mode network activity by acute tryptophan depletion is associated with mood change: a resting state functional magnetic resonance imaging study. Neurosci Res 69: 129–134.
86. van Wingen GA, Tendolkar I, Urner M, van Marle HJ, Denys D, et al. (2013) Short-term antidepressant administration reduces default mode and task-positive network connectivity in healthy individuals during rest. Neuroimage 88C: 47–53.
87. Hardwick RM, Rottschy C, Miall RC, Eickhoff SB (2013) A quantitative meta-analysis and review of motor learning in the human brain. Neuroimage 67: 283–297.
88. Kraus C, Ganger S, Losak J, Hahn A, Savli M, et al. (2013) Gray matter and intrinsic network changes in the posterior cingulate cortex after selective serotonin reuptake inhibitor intake. Neuroimage 84C: 236–244.
89. Posner J, Hellerstein DJ, Gat I, Mechling A, Klahr K, et al. (2013) Antidepressants normalize the default mode network in patients with dysthymia. JAMA Psychiatry 70: 373–382.
90. Murphy DL, Fox MA, Timpano KR, Moya PR, Ren-Patterson R, et al. (2008) How the serotonin story is being rewritten by new gene-based discoveries principally related to SLC6A4, the serotonin transporter gene, which functions to influence all cellular serotonin systems. Neuropharmacology 55: 932–960.
91. Alasaari JS, Lagus M, Ollila HM, Toivola A, Kivimaki M, et al. (2012) Environmental stress affects DNA methylation of a CpG rich promoter region of serotonin transporter gene in a nurse cohort. PLoS One 7: e45813.
92. van IMH, Caspers K, Bakermans-Kranenburg MJ, Beach SR, Philibert R (2010) Methylation matters: interaction between methylation density and serotonin transporter genotype predicts unresolved loss or trauma. Biol Psychiatry 68: 405–407.
93. Olsson CA, Foley DL, Parkinson-Bates M, Byrnes G, McKenzie M, et al. (2010) Prospects for epigenetic research within cohort studies of psychological disorder: a pilot investigation of a peripheral cell marker of epigenetic risk for depression. Biol Psychol 83: 159–165.
94. Kinnally EL, Tarara ER, Mason WA, Mendoza SP, Abel K, et al. (2010) Serotonin transporter expression is predicted by early life stress and is associated with disinhibited behavior in infant rhesus macaques. Genes Brain Behav 9: 45–52.
95. El-Kasaby A, Just H, Malle E, Stolt-Bergner PC, Sitte HH, et al. (2010) Mutations in the carboxyl-terminal SEC24 binding motif of the serotonin transporter impair folding of the transporter. J Biol Chem 285: 39201–39210.
96. Bruchas MR, Schindler AG, Shankar H, Messinger DI, Miyatake M, et al. (2011) Selective p38alpha MAPK deletion in serotonergic neurons produces stress resilience in models of depression and addiction. Neuron 71: 498–511.
97. Carneiro AM, Cook EH, Murphy DL, Blakely RD (2008) Interactions between integrin alphaIIbbeta3 and the serotonin transporter regulate serotonin transport and platelet aggregation in mice and humans. J Clin Invest 118: 1544–1552.
98. Drevets WC, Price JL, Simpson JR, Jr., Todd RD, Reich T, et al. (1997) Subgenual prefrontal cortex abnormalities in mood disorders. Nature 386: 824–827.
99. Mayberg HS, Lozano AM, Voon V, McNeely HE, Seminowicz D, et al. (2005) Deep brain stimulation for treatment-resistant depression. Neuron 45: 651–660.